IET Electric Power Applications

*Research Article*

IET Journals
The Institution of Engineering and Technology

# Stator inter-turn faults diagnosis in induction motors using zero-sequence signal injection

ISSN 1751-8660
Received on 4th June 2020
Revised 27th October 2020
Accepted on 6th November 2020
doi: 10.1049/iet-epa.2020.0461
www.ietdl.org

*Marcial Otero*[1] ✉, *Pablo M. de la Barrera*[1], *Guillermo R. Bossio*[1], *Roberto Leidhold*[2]

[1]*Research Institute for Energy Technologies and Advanced Materials (IITEMA), National University of Rio Cuarto, Rio Cuarto, Argentina*
[2]*Institute of Electric Power Systems (IESY), Otto-von-Guericke-Universität Magdeburg, Magdeburg, Germany*
✉ *E-mail: motero@ing.unrc.edu.ar*

**Abstract:** This study presents a strategy for stator inter-turn faults diagnosis in induction motors (IMs) operating under time-variable load and time-variable speed conditions. The strategy consists in injecting a zero-sequence high-frequency signal in order to analyse variations in the stator inductances. Incipient stator inter-turn faults are detected by a simple signal processing of the derivatives of the currents. A feature of the strategy is that the zero-sequence high-frequency signal is generated by the inverter that feeds the machine, without modifying the standard space vector modulation of the IM-drive. Experimental results show that faults representing <1% of the stator winding can be detected, as well as the phase location of the fault, validating this proposal.

## 1 Introduction

Industrial processes are always pursuing to satisfy efficiency requirements, mainly considering low cost and high reliability. Induction motors (IMs) are the most widely used machines related to industrial processes [1], and eventual failures in these machines may lead to severe economic losses, related to the repair costs and the eventual production downtimes. For these reasons, many efforts have been made to increase the reliability of IM by means of faults diagnosis (FD) at incipient stages [2].

IM faults can be classified in rotor, stator and mechanical related faults, including bearing faults and air gap eccentricity. Almost 37% of the IM faults are related to insulation problems, leading to a short-circuit fault [3]. One of the most common stator faults is inter-turn fault (ITF), which appears as a consequence of the degradation of the stator windings insulation [4]. This degradation can be caused by thermal, electrical, mechanical and/or environmental stresses.

As a result of an ITF, the current density in the faulty turns increases over the rated values causing a hot spot area around them [5]. Therefore, an incipient ITF could accelerate the insulation degradation of the windings, leading to more severe faults in the IM. Fig. 1 shows an industrial case of a severe ITF in a 55 kW IM, which was driving a water pump in a thermal power station. ITFs are irreversible and they are considered the most destructive faults in rotational electrical machines [6]. For this reason, different FD strategies have been developed for the detection and diagnosis of incipient ITF [7].

ITF detection and diagnosis strategies can be classified in passive and active approaches. The former analyse the response of the machine when it is excited by fundamental components of the electric variables intended to produce torque. The latter consist in the injection of an additional signal in the machine and further analysis of its response.

**Fig. 1** *ITF in a 55 kW induction motor*

Some of the most well-known passive fault diagnosis approaches are the motor current signature analysis [8], instantaneous active and reactive power signature analysis [9, 10], model-based strategies [11, 12], stray flux analysis [13] and the use of artificial intelligence approaches [14, 15]. Most of these FD strategies have the disadvantage that they can be sensitive to the variations on the amplitude or frequency of the fundamental components of the electric variables, being therefore sensitive to variations in the operation points of the machine, mainly for a time-variable load or a time-variable speed conditions. Also, some of these strategies require previous knowledge of the healthy machine, e.g. the reference current signature or detailed model parameters.

An important challenge has been the ITF diagnosis in closed-loop inverter-fed machines, where the control loop tends to hide the faults [16]. In this scenario, the conventional FD strategies have some difficulties to reach good results. Active fault diagnosis (AFD) approaches pursue to overcome the limitations of the conventional FD proposals. The signal injection at particular frequencies can increase the detectability of some faults, making the technique more sensitive for an incipient FD. The AFD becomes more interesting for its application in closed-loop drives, mainly for two reasons. On the one hand, the signal injection technique can be designed to be applied by the inverter that feeds the machine. On the other hand, the injected signals can overcome the hiding effect of the closed-loop control on the fault signals, because AFD strategies do not rely on the fundamental components of the electric variables, but on the response to the injected signals. In spite of the AFD advantages, the signal injection techniques can produce torque pulsations or additional losses in the machine [17].

Among the signal injection techniques, high frequency (HF) signals have been used for the detection of those faults that produce modifications in the magnetic couplings of the machine, as airgap eccentricity [18], broken rotor bars [19] or winding faults [20]. Some methods are based on the rotating or pulsating-type HF signal injection superimposed on the controller command voltage [20–24], others apply inherent HF components of the drive pulse width modulation (PWM), shortly modifying the modulation to inject predefined switching vectors [24–27]. Other proposals have used inherent PWM switching harmonics to replace the injected signal, avoiding the modulation modification [28, 29].

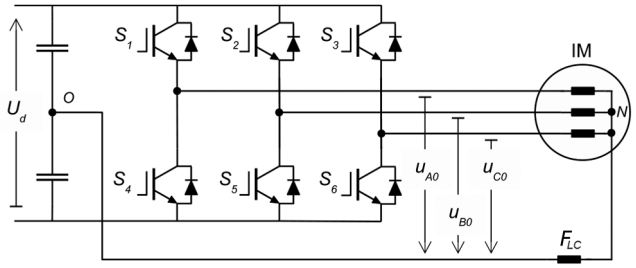


**Fig. 2** *Standard inverter used for signal injection*

**Table 1** Passive band-pass filter parameters

| *L*, mH | *C*, μF | Resonance frequency, kHz |
|---|---|---|
| 12 | 1 | 1.45 |

The saliencies of the machine are usually analysed in order to detect and identify an ITF. The main drawbacks of the techniques that superimposed a HF signal injection are frequency limitation of injection (usually no more than 1/5 of the switching frequency) and some related acoustic emissions. Besides, in most of them, some portion of the total DC-link voltage is used to inject the additional signal, which limits the speed range of application of the diagnosis technique. The techniques based on modifying the PWM have the weakness of requiring extra inverter-switching operations, which increase the switching losses and can compromise the insulation because of possible partial discharges caused by the commutations. Another aspect is that these proposals increase the control technique complexity. The techniques based on the switching harmonics analysis require some extra signal processing, in order to identify and remove the variations of the PWM ripple current under healthy operation with varying speeds and loading, accomplishing in this way an accurate ITF diagnosis.

In [24], two HF signal injection techniques, previously used for saliency tracking of permanent magnet synchronous machines (PMSM), are used for ITF diagnosis. The evaluation is based on comparing a saliency reference, generated by an algorithm, with the saliency signals obtained by the signal injection. The variations in the error of this comparison were then used for fault detection. The two evaluated and compared techniques were HF rotating voltage injection and the INFORM method, the latter interrupts the normal PWM pattern for the application of the testing vectors. The experimental results present ITF detection for PMSM under time-varying speed conditions at constant load. Moreover, both techniques are suitable for ITF diagnosis at zero speed condition. The main drawback of these techniques is that they rely on a precise knowledge of the saliencies of the machine as reference.

The AFD techniques based on the analysis of negative-sequence currents have also reached interesting results. In [21], an AFD technique for ITF diagnosis in IM was presented, which consists of modifying the inverter modulation in order to inject a HF rotating voltage. This technique was based on detecting the fixed imbalance that an ITF generates on the stator transient inductances. Severity and phase location of the ITF are detected, for different stationary load conditions and for different frequencies of the fundamental excitation. Among the aforementioned disadvantages of injecting an additional rotating signal, this technique required adjusting the number of samples used for the processing according to the fundamental frequency.

Detecting ITF in IM operating at time-variable load and time-variable speed conditions without modifying the PWM has been a difficult task, and it is a subject on which few contributions have been found in the consulted bibliography. This paper proposes a zero-sequence signal injection strategy for stator ITF diagnosis on a closed-loop inverter-fed IM, with low sensitivity to time-variable load and time-variable speed conditions. A similar strategy was used for the detection of ITFs [30] and broken bars [31, 32] in IM operating under stationary conditions. It is well known that an ITF modifies the inductances of the IM [33, 21], the proposed technique detects these variations without modifying the standard space-vector modulation (SVPWM) using a simple signal processing. The signal injection strategy used in this effort has to be discerned from zero-sequence voltage measurement as in [29, 34]. In [29], the sideband response of the PWM switching harmonics in common-mode voltage is processed and analysed for ITF diagnosis, applying conjugation and subtraction operations to switching sidebands. In [34], a carrier signal is injected in the non-homopolar ($\alpha\beta$ or $dq$) components, which interacts with the current controller, while the response is analysed on the zero-sequence voltage. In this paper, the carrier is injected in the zero-sequence and the response is analysed in the non-homopolar current components ($\alpha\beta$). The zero-sequence carrier has the advantage that it does not interact with the current controller.

In addition, in this paper ITFs representing <1% of the stator windings are detected, and the phase location of the ITF is achieved. Reliably detecting very low severity faults has been demonstrated to be a difficult issue to asses [35], and it is an important characteristic of the strategy presented in this work. Experimental results with the machine operating at time-variable load and time-variable speed conditions are presented, demonstrating the effectiveness of the strategy. A limitation of this technique is that it requires access to the neutral point of the machine, but accessing the neutral point has been proved to be useful for sensorless rotor position estimation [34, 36] and fault tolerant strategies [37]. The proposed topology, which requires a connection of the neutral point with the middle of the DC-link, has already been used for rotor position estimation [38] and shows some advantages for common-mode current reduction [39].

This paper is organised as follows. Section 2 presents the zero-sequence signal injection strategy, the experimental setup as well as obtained results are presented in Section 3. Section 4 presents a fault detection and isolation (FDI) method. Finally, some conclusions and final remarks are drawn in Section 5.

## 2 Zero-sequence signal injection strategy

The strategy for stator ITF diagnosis is presented in this section. It is based on the analysis of the current derivatives of the stator when a zero-sequence HF signal is injected to the motor. A study of the influence of ITF on the values of the stator current derivatives is performed for the diagnosis.

The IM is fed by a three-phase inverter using SVPWM, which applies the active voltage vectors $\boldsymbol{u}_1$ to $\boldsymbol{u}_6$ and the zero vectors $\boldsymbol{u}_0$ and $\boldsymbol{u}_7$ as described in [40]. The states $u_0$ and $u_7$ are alternately applied on each cycle of the SVPWM. These zero vectors produce a zero-sequence voltage at switching frequency which, however, has no effect on the currents while the neutral point is disconnected. As this voltage will be used as injected signal, the neutral point has to be connected to the DC-link midpoint.

A diagram of the inverter and the IM connection is presented in Fig. 2. The IM is used with a star connection, where the neutral point ($N$) is connected to the middle of the DC-link ($O$) through a band-pass filter ($F_{\mathrm{LC}}$). The SVPWM also produces an intrinsic low frequency zero-sequence voltage, which would create high currents on the neutral point connection, leading to additional losses in the machine and torque pulsations. In order to overcome these issues, the band-pass filter is placed in the connection, offering high impedance for up to six times the highest fundamental frequency, and lower impedance for the switching frequency. This reduces the impact of the strategy in the motor currents and torque. The signal is injected without interacting with the current control that runs in the non-zero-sequence ($dq$). The filter parameters are shown in Table 1.

During the state $u_7$ ($S_1$, $S_2$ and $S_3$ switched on, in Fig. 2), the voltage on the IM with respect to the point $O$ is

$$\begin{bmatrix} u_{A0}^{7} & u_{B0}^{7} & u_{C0}^{7} \end{bmatrix}^{\mathrm{T}} = \boldsymbol{M}\frac{U_d}{2} \tag{1}$$

while, for state $u_0$ ($S_4$, $S_5$ and $S_6$ on) is

$$\begin{bmatrix} u_{A0}^{0} & u_{B0}^{0} & u_{C0}^{0} \end{bmatrix}^{\mathrm{T}} = -\boldsymbol{M}\frac{U_d}{2} \tag{2}$$

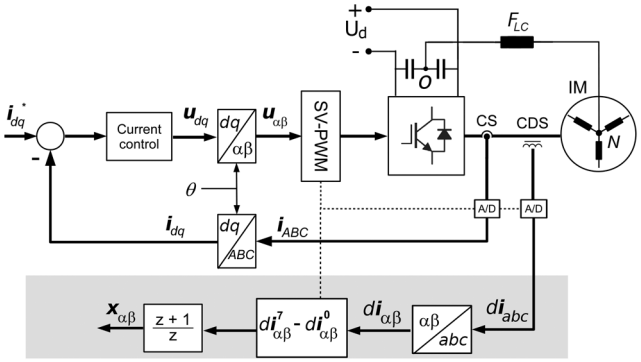


**Fig. 3** *Block diagram of the signal injection strategy and signal processing*

where $\boldsymbol{M} = [1 \quad 1 \quad 1]^{\mathrm{T}}$ and $U_d$ is the DC-link voltage. This paper studies the effect of the HF zero-sequence signal injection in the IM, using the simplified model of the IM presented in [41]. It proposes that it is possible to model each phase of the stator as an arrangement of resistances ($\boldsymbol{R}$), coupling inductances which depend on the position of the rotor ($\boldsymbol{L}(\theta_r)$), and the electromotive force (EMF) which depends on the motor speed ($\boldsymbol{e}(\omega_r)$).

Based on this model, when the $u_7$ state is applied, the IM can be represented by the following equation:

$$\boldsymbol{L}_{\mathrm{abc}}(\theta_r)\frac{\mathrm{d}}{\mathrm{d}t}\boldsymbol{i}^{7}_{\mathrm{abc}} = -\boldsymbol{R}_{\mathrm{abc}}\boldsymbol{i}^{7}_{\mathrm{abc}} - \boldsymbol{e}(\omega_r) + \boldsymbol{M}\frac{U_d}{2} \tag{3}$$

and for the $u_0$ state

$$\boldsymbol{L}_{\mathrm{abc}}(\theta_r)\frac{\mathrm{d}}{\mathrm{d}t}\boldsymbol{i}^{0}_{\mathrm{abc}} = -\boldsymbol{R}_{\mathrm{abc}}\boldsymbol{i}^{0}_{\mathrm{abc}} - \boldsymbol{e}(\omega_r) - \boldsymbol{M}\frac{U_d}{2} \tag{4}$$

where $\boldsymbol{i}_{\mathrm{abc}}$ is the vector of phase currents, and the subscripts abc refer to each stator phase. The third terms on the right hand of (3) and (4) are the phase voltages of the IM during $\mathrm{u}_0$ and $\mathrm{u}_7$ states, respectively.

The current derivatives, modelled in (3) and (4), cannot be directly used for condition monitoring of the IM because they do not depend only in the inductances of the machine, but also on the resistive voltage drop and the EMF. The current derivatives are measured every two consecutive null states, meaning every 100 $\mu$s considering a 5 kHz switching frequency. Therefore, it is possible to assume that the resistive voltage drop and the EMF do not change much between the two samples, taken at $\mathrm{u}_0$ and at $\mathrm{u}_7$, which is why a signal independent of these values can be obtained using the difference between each inverter state. Considering (3) and (4), it yields

$$\frac{\mathrm{d}}{\mathrm{d}t}\boldsymbol{i}^{7}_{\mathrm{abc}} - \frac{\mathrm{d}}{\mathrm{d}t}\boldsymbol{i}^{0}_{\mathrm{abc}} \cong \boldsymbol{L}^{-1}_{\mathrm{abc}}\boldsymbol{M}U_d \tag{5}$$

Transforming the variables to the $\alpha\beta 0$ reference frame

$$\frac{\mathrm{d}}{\mathrm{d}t}\boldsymbol{i}^{7}_{\alpha\beta 0} - \frac{\mathrm{d}}{\mathrm{d}t}\boldsymbol{i}^{0}_{\alpha\beta 0} = \boldsymbol{L}^{-1}_{\alpha\beta 0}\begin{bmatrix}0\\0\\1\end{bmatrix}U_d \tag{6}$$

where

$$\boldsymbol{L}^{-1}_{\alpha\beta 0} = \begin{bmatrix} Y_{\alpha\alpha} & Y_{\alpha\beta} & Y_{\alpha 0} \\ Y_{\beta\alpha} & Y_{\beta\beta} & Y_{\beta 0} \\ Y_{0\alpha} & Y_{0\beta} & Y_{00} \end{bmatrix} \tag{7}$$

replacing (7) in (6)

$$\begin{bmatrix}\frac{\mathrm{d}}{\mathrm{d}t}i^{7}_{\alpha}\\ \frac{\mathrm{d}}{\mathrm{d}t}i^{7}_{\beta}\\ \frac{\mathrm{d}}{\mathrm{d}t}i^{7}_{0}\end{bmatrix} - \begin{bmatrix}\frac{\mathrm{d}}{\mathrm{d}t}i^{0}_{\alpha}\\ \frac{\mathrm{d}}{\mathrm{d}t}i^{0}_{\beta}\\ \frac{\mathrm{d}}{\mathrm{d}t}i^{0}_{0}\end{bmatrix} = \begin{bmatrix}Y_{\alpha 0}\\ Y_{\beta 0}\\ Y_{00}\end{bmatrix}U_d \tag{8}$$

The first two rows of (8) will be used in this paper as diagnostic signals for ITF diagnosis, and can be rewritten as follows:

$$x_{\alpha} = \frac{\mathrm{d}}{\mathrm{d}t}i^{7}_{\alpha} - \frac{\mathrm{d}}{\mathrm{d}t}i^{0}_{\alpha} = Y_{\alpha 0}U_d \tag{9}$$

$$x_{\beta} = \frac{\mathrm{d}}{\mathrm{d}t}i^{7}_{\beta} - \frac{\mathrm{d}}{\mathrm{d}t}i^{0}_{\beta} = Y_{\beta 0}U_d \tag{10}$$

These signals only depend on the DC-link voltage and the inductances of the IM. Therefore, it is possible to assert that changes in the IM inductances, as a consequence of ITFs, can be detected by processing the diagnostic signals $x_{\alpha}$ and $x_{\beta}$.

A block diagram of the proposed zero-sequence signal injection strategy is shown in Fig. 3. In the upper part, a scheme of a standard drive is shown. The current control defines the modulation based on the references of the flux related ($i_d$) and torque related ($i_q$) current components. The current derivatives are measured by three current-derivative sensors (CDS). The AD converters are synchronised with the PWM in order to acquire the signals in the middle of $\mathrm{u}_0$ and $u_7$ states, that are the usual sampling points for the current control. The shadowed area of the diagram shows the signal processing. The signals are transformed to the $\alpha\beta$ reference frame. Then, from two consecutive samples, those taken at state $\mathrm{u}_0$ are subtracted from those taken at state $\mathrm{u}_7$, to obtain the diagnostic signals ($\boldsymbol{x}_{\alpha\beta}$) as in (9) and (10). Finally, the signals $\boldsymbol{x}_{\alpha\beta}$ are passed by a low-pass filter. These signals will be analysed in the next section, where experimental results are presented, in order to obtain information about the IM stator condition.

## 3 Experimental setup and results

The proposed strategy for condition monitoring of IM was implemented in a test-bench, based on the block diagram of Fig. 3, with a DC-link voltage ($U_d$) of 580 V. The field oriented control and the proposed method were implemented with an ×86-based PC, running the real-time operating system Linux-RTAI. A self-developed PCI interface implements the standard SVPWM and A/D conversions. The control algorithm has a sampling frequency of 10 kHz, and an inverter switching frequency of 5 kHz. Although the strategy was programmed on a PC, it has a low computational requirement. For this reason, it can be easily implemented in a microcontroller of a standard variable speed drive (VSD). A picture of the overall experimental setup is presented in Fig. 4. The components of the setup are listed in Table 2.

The strategy was tested on a standard IE2 5.5 kW IM, whose rated variables and constructive features are provided in Table 3. The motor was modified in order to access different points of a coil, where it is possible to make ITFs of different severities. Fig. 5 shows the test rig, where the access to the stator windings can be seen. A low voltage circuit breaker is located outside the motor frame, to manually make the ITF during the tests. The only fault resistance ($R_{\mathrm{f}}$) considered is the lead connecting the circuit breaker with the stator winding access. The windings distribution is shown in Figs. 6*a* and *b*.

In order to obtain the diagnostic signals, the current derivatives must be measured or calculated, in this work they were obtained by self-developed CDS, presented and described in Fig. 7. The implemented CDS are formed by one simple high-frequency transformer for each phase, for isolated measurement. The secondary voltage is proportional to the current derivative of the primary [42].

The use of additional sensors is usually undesirable, because it requires extra connections and represents additional costs. Using the currents signals, already acquired for control purposes, could be

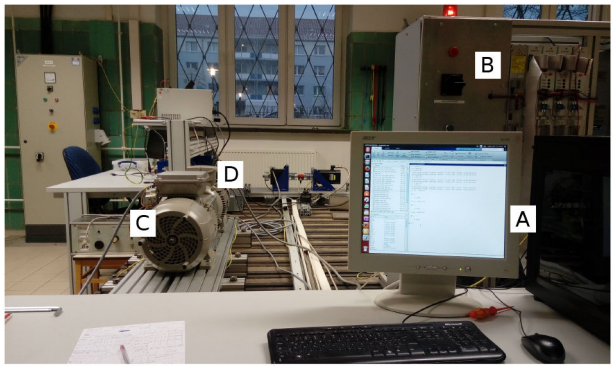


**Fig. 4** *Experimental setup. Figure description is in Table 2*

**Table 2** Overall experimental setup description

| Notation | Component | Description/purpose |
|---|---|---|
| A | desktop PC | control and signal acquisition |
| B | power cabinet and inverters | one inverter for each motor |
| C | IE2 5.5 kW IM | modified to make ITF |
| D | IE3 5.5 kW IM | used for speed control |

**Table 3** IM rated variables and constructive features

| Variable/parameter | Value | Unit |
|---|---|---|
| power ($P_n$) | 5.5 | kW |
| line voltage ($V_n$) | 380 | Vrms |
| rated current ($I_n$) | 11.9 | Arms |
| frequency ($f_n$) | 50 | Hz |
| power factor | 0.80 | — |
| poles ($P$) | 4 | — |
| number of stator slots | 36 | — |
| number of rotor slots | 28 | — |
| number of turns per stator phase | 168 | — |
| stator phase resistance ($R_s$) | 1.4 | Ω |
| stator phase leakage inductance ($L_{ls}$) | 10.4 | mH |

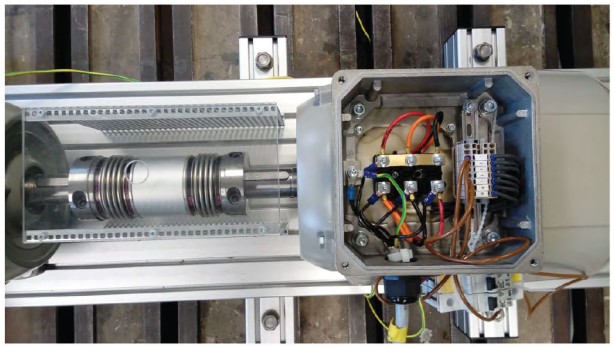

**Fig. 5** *Test rig. IM with special winding to make ITFs, coupled to an IM with speed control*

an option. Doing this would require to take at least the difference of two current samples ($\Delta i$) within a time interval ($\Delta t$), leading to $di/dt \simeq \Delta i/\Delta t$. According to [43], this method would need much higher resolution of the analogue-to-digital conversion, since small differences of high amplitude values must be transmitted. It is worth to mention the simplicity and low cost of the proposed CDS, which does not need any active electronic component. Also, using additional sensors to specifically measure HF signals can provide very good sensitivity on this task [44] and higher signal-to-noise ratio [42]. The use of the proposed strategy can be justified for machines operating on critical applications, such as electrical vehicles, or driving critical loads.

For the proposed signal injection strategy, the switching frequency of the inverter determines the frequency of the zero-

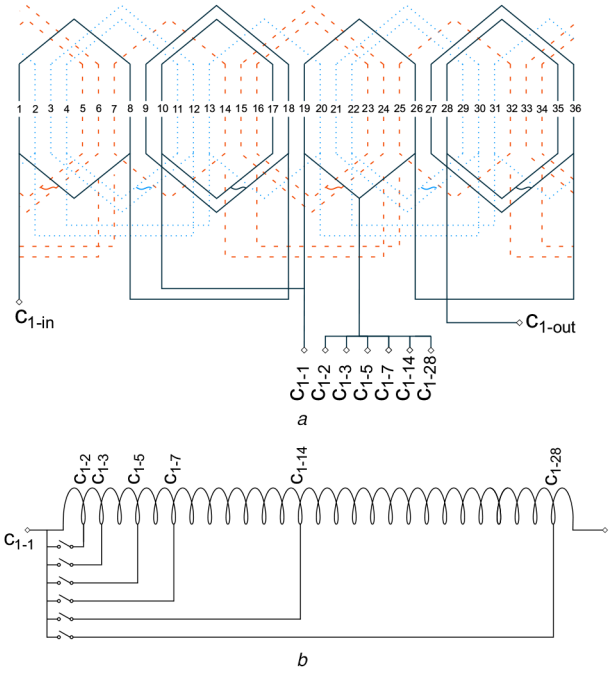


**Fig. 6** *Description of the stator windings of the IM*
***(a)*** Winding distribution of stator phases, ***(b)*** Stator coil with different outputs

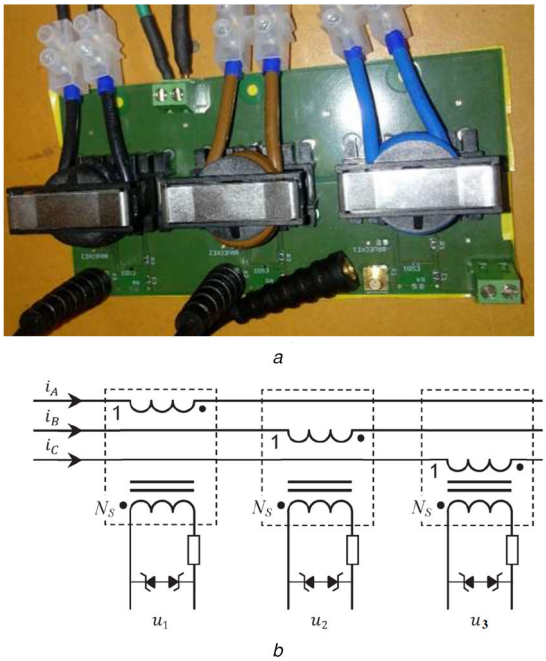


**Fig. 7** *Self-developed current-derivatives sensors*
***(a)*** Picture of the self-developed CDS, ***(b)*** Scheme of the self-developed CDS

sequence injected signal, being the zero vectors of the SVPWM. In the present work, a frequency of 5 kHz was selected, which is one of the most recommended frequencies for commercial VSD [45]. It is well known that higher frequencies can be used, and for the proposed strategy employing a higher switching frequency would provide better resolution to the diagnostic signals, but with some possible drawbacks. First, increasing the switching frequency can compromise the stator winding insulation, because of the increase on the voltage spikes caused by the commutations [46, 47]. Second, the current derivative is sampled between the switching events of the inverter, while the signal is almost constant. During the switching itself, the current derivative may present high peaks that must not be measured. If the switching frequency is increased, the time available for a correct signal acquisition gets smaller. Therefore, increasing the switching frequency could make the

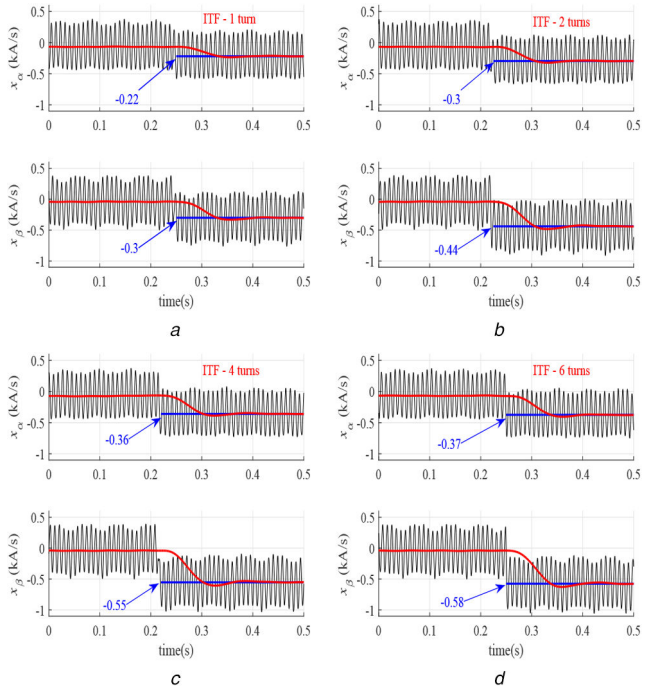


**Fig. 8** *Diagnostic signals for different ITF severities at* $\omega_r = 240\,\mathrm{r/min}$
***(a)*** ITF of 1 turn, ***(b)*** ITF of 2 turns, ***(c)*** ITF of 4 turns, ***(d)*** ITF of 6 turns

**Table 4** Euclidean norm of the diagnostic signal for different fault severities

| Index | Healthy | ITF-number of turns | | | |
|---|---|---|---|---|---|
| | | 1(0.6%) | 2 | 4 | 6 |
| $\| \boldsymbol{x}_{\alpha\beta} \|$ kA/s | 0.08 | 0.37 | 0.53 | 0.66 | 0.69 |

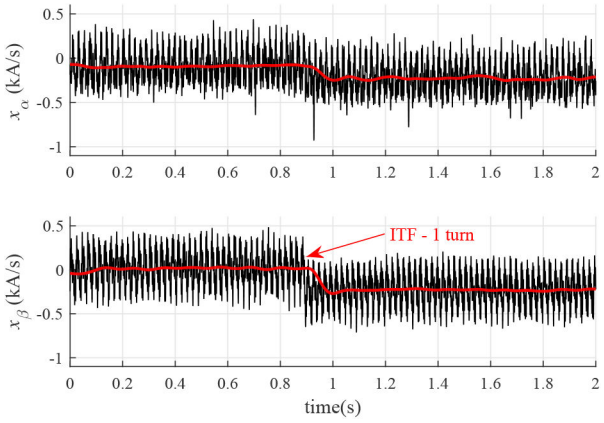


**Fig. 9** *Diagnostic signals behaviour for the IM operating at* $\omega_r = 60\,\mathrm{r/min}$

strategy application more complex and also require a faster signal acquisition.

With the objective of analysing the effectiveness of the IM ITF diagnosis strategy several experimental results were obtained, for different ITF severities and for an IM operating under different load and speed conditions.

### *3.1 Experimental results for different ITF severities*

The results presented in Fig. 8 show the behaviour of the diagnostic signals under different fault severities. These experiments were made with the IM operating at a constant speed of $\omega_r = 240\,\mathrm{r/min}$, rated flux ($i_d = 6.5\,\mathrm{A}$) and no load ($i_q = 0\,\mathrm{A}$). These figures show the diagnostic signals as function of the time during two revolutions of the IM. In the first time segment of the test, the IM is operating in healthy condition and in the second one it is under fault.

According to [30], the diagnostic signals have a sinusoidal shape with 28 cycles per revolution of the rotor, corresponding to the number of rotor bars. In addition, four cycles per revolution component related to the rotor flux is also reported in the cited paper and shown in Fig. 8.

In the middle of the test time, an ITF is applied to the phase *C* of the stator. As a consequence, an important mean value is observed in the diagnostic signals presented in the figures. This mean value is indicated with a blue line. A red line is also presented, which corresponds to the result of applying a low-pass filter to the diagnostic signals. The mean value for the healthy condition is different to zero as a consequence of inherent asymmetries of the IM. In addition, the high sensitivity of the proposed ITF diagnosis strategy is observed in Fig. 8*a*, where even an ITF of a single turn is detected. It is worth mentioning that each stator phase has a total of 168 turns, therefore a single turn represents 0.6% of the total IM stator winding.

The sensitivity of the strategy can be quantified by using the Euclidian norm of the diagnostic signal mean value ( $\| \boldsymbol{x}_{\alpha\beta} \|$ ). For the healthy condition $\| \boldsymbol{x}_{\alpha\beta} \| = 0.08\,\mathrm{kA/s}$ and for an ITF of one turn $\| \boldsymbol{x}_{\alpha\beta} \| = 0.37\,\mathrm{kA/s}$. The same behaviour is observed for other results in Figs. 8*b–d*, and it is remarkable how the mean value increases with the fault severity. Table 4 shows the variation of the Euclidean norm for different fault severities. The fault severity is easily identified when the short circuit involves a small number of turns. However, if a big amount of turns are involved it gets harder to estimate the fault severity. When an ITF occurs, the self- and mutual-inductance of the phases and the short-circuited turns present a non-linear variation with the fault severity. This effect produces a non-linear relationship between the fault indicator and the number of short-circuited turns. These results agree with those reported in [30] and it is a behaviour also shown in other AFD proposals [24, 27]. Therefore, the next sections deal with the validation of the proposal for different IM working conditions, e.g. different speed and load torque as well as time-variable speed conditions.

### *3.2 Experimental results for different load and speed conditions*

Fig. 9 shows the result of detecting an ITF for the IM with speed fixed at $\omega_r = 720\,\mathrm{r/min}$, and operating with 50% of the rated load. Analysing the diagnostic signals it can be observed that as a consequence of this load, the four cycles/rev component increases its value comparing it with previous tests. It is worth mentioning that for the healthy case the mean value is not significantly affected by the load condition.

In the test of Fig. 9, a one-turn ITF is introduced at 0.9 s. The figure clearly shows how the mean values of the diagnostic signals increase as a consequence of the fault. This can be observed by analysing the value of the filtered signal, which is shown in red.

In Fig. 10, the IM operates at $\omega_r = 60\,\mathrm{r/min}$, and with 50% load. Approximately, at 2.6 s an ITF is applied and, as a consequence, a mean value arises on the diagnostic signals. It is worth mentioning that the flux component of the signal is at 2.6 cycles/rev, instead of at 4 cycles/rev as in Fig. 8, due to the effect of the slip caused by the load condition [30]. Taking this fact into account, it can be noticed that the mean value, presented by the filtered signal, takes almost 0.8 s to achieve the steady state and, therefore, the fault detection gets slower.

This effect was also present in the results shown in Fig. 9, nevertheless, it did not affect considerably the fault detection time due to the fact that the speed was higher. Namely, the fault detection time increases when the rotor speed decreases.

In spite of the fact that the strategy takes more time to detect the fault for the IM operating at lower speeds, this would not endanger the integrity of the IM. It is known that for an inverted-fed IM the current on the short-circuited turns decreases considerably at lower speeds. Using the transient model of the IM proposed in [48], this current can be calculated for different speeds as

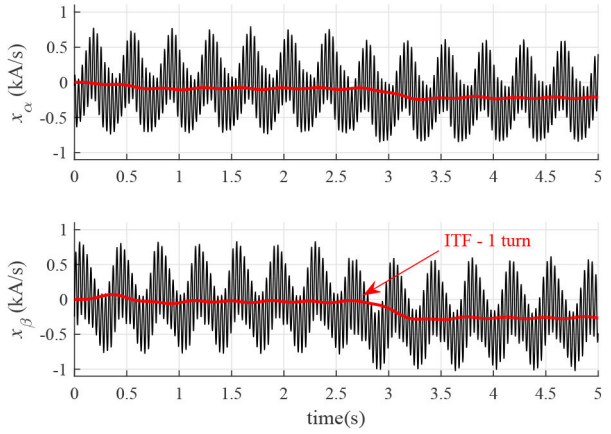


**Fig. 10** *Diagnostic signals behaviour for the IM operating at* $\omega_r = 720\,\mathrm{r/min}$

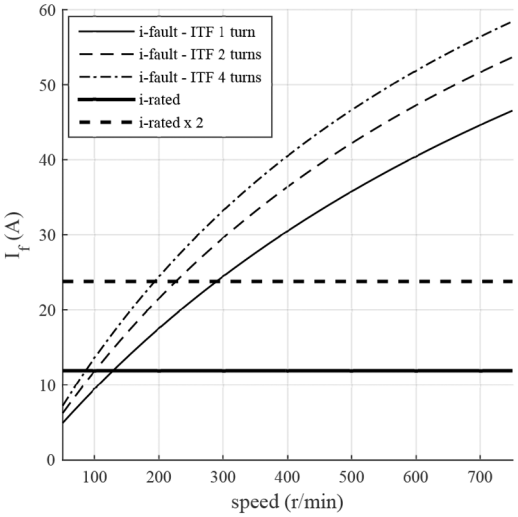


**Fig. 11** *Variation of the faulty turns current with the speed*

**Table 5** Current under different operating conditions for an ITF of 1 turn

| Current | $\omega = 240\,\mathrm{r/min}$ | $\omega = 360\,\mathrm{r/min}$ | $\omega = 720\,\mathrm{r/min}$ |
|---|---|---|---|
| stator current, A | 7.5 | 7.5 | 7.6 |
| ITF short current, A | 18.2 | 25.6 | 48.8 |

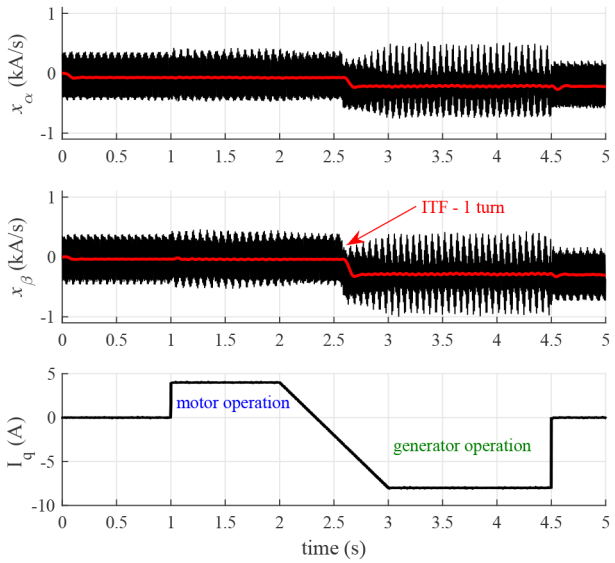


**Fig. 12** *Diagnostic signals for the IM operating at time-variable* $i_q$

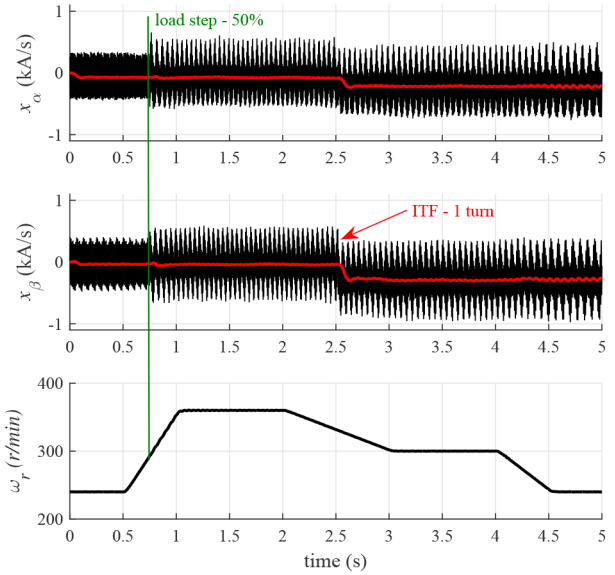


**Fig. 13** *Diagnostic signals behaviour for the IM operating at time-variable speed and variable load*

$$i_{\mathrm{f}} = \frac{\mu(U_n/f_n)f}{\mu(1-2(\mu/3))(R_s + 2\pi f L_{\mathrm{ls}}) + R_{\mathrm{f}}} \tag{11}$$

where $i_{\mathrm{f}}$ is the current in the faulty turns in Amperes, $\mu$ is the percentage of the winding under ITF, $U_n$ and $f_n$ are the rated voltage and frequency of the machine, $f$ is the applied frequency according to the IM speed, $R_s$ is the per-phase resistance, $L_{ls}$ the per-phase leakage inductance and $R_{\mathrm{f}}$ the fault resistance. In addition, $i_{\mathrm{f}}$ is calculated only considering the positive-sequence voltage.

Considering our particular test-bench, different fault current values were obtained applying (11). The IM parameters presented in Table 3 were used, with a fault resistance $R_{\mathrm{f}} = 6\,\mathrm{m\Omega}$, which corresponds to the resistance of a 2.5 $\mathrm{mm}^2$ commercial lead of 0.8 m long. The fault current values are presented in Fig. 11. The figure shows the results for three different fault severities and also the rated current of the IM, in a range of speeds from 50 to 750 r/min. Some experimentally obtained currents are listed in Table 5.

From Fig. 11 it is possible to see how the fault current increases dangerously for high speed. Also, the fault current does not represent a big risk to the integrity of the windings for speeds lower than 100 r/min. Therefore, the fault will not be degenerative below that speed, providing more time to detect ITF at an incipient stage.

Fig. 12 shows a test for the IM operating under load variation, starting with no load and applying a step load of 25% at 1 s. From 2 to 3 s, another variation of the load is applied, passing from motor operation to generator operation. The IM operates 1.5 s at 50% of load as generator, and on the last half second of the test the load is removed. All this can be seen looking at the $i_q$ current. It is shown how the load variation affects the amplitude of the diagnostic signals but not the mean value, which only shows a variation when an ITF on the windings is produced, nearly at 2.6 s.

The validity of the proposal was demonstrated in Figs. 9, 10 and 12 for different constant speeds. Fig. 13 shows the effectiveness of the proposal under speed variations, changing from 240 to 360 r/min, then to 300 r/min and finally back to 240 r/min. Starting with no load, at 0.7 s a load step of 50% is applied. At 2.5 s, when the speed is changing, an ITF is produced. Looking at $x_\alpha$ and $x_\beta$, it can be noticed a mean value arising only as a consequence of the fault.

## 4 Fault detection and isolation method

This section presents an FDI method for the ITF diagnosis. Fig. 14 shows several points in the $\alpha\beta$-plane, corresponding to different experimental results. Each point distance to (0,0) is calculated by the Euclidean norm $\| \boldsymbol{x}_{\alpha\beta} \|$ and its angle as

$$\theta_{\boldsymbol{x}_{\alpha\beta}} = \text{atan2}\left(\bar{x}_\beta, \bar{x}_\alpha\right). \quad (12)$$

Results for different ITF severities and locations for the IM operating at different load conditions are presented. A total of 14 results are shown in Fig. 14, from which five correspond to healthy cases and nine to faulty cases. All the tests marked with circles were made at constant speed of 240 r/min, with the IM operating under no load condition and with the $i_d$ current fixed at the rated value of 6.5 A. All the faulty cases correspond to the IM used in the previously presented experimental results (see Table 3). Looking at the displacements corresponding to the faulty cases, it is visible on the figure how the value of $\| \boldsymbol{x}_{\alpha\beta} \|$ increases with the fault severity, and it can also be observed that the direction of the displacement of the points is related with the faulty phase.

A 'healthy zone' is drawn in the figure, which is useful to define the difference between a healthy motor and a faulty one, even when there is no previous reference of the condition of the machine. An ideal value of a healthy case would point out that each point corresponding to a healthy IM should be located in (0,0), but this does not happen because of slight asymmetries of the motor that can be related to the construction process. The faulty cases present 1, 2 and 4 ITF severities for each phase of the IE2 IM. The difference between the healthy cases and the faulty ones is remarkable, showing the accuracy and sensitivity of the proposed ITF diagnosis strategy.

Inside the healthy zone, five results can be compared. Three different motors were tested under this condition. The healthy cases correspond to the 5.5 kW IE2 IM, described in Table 3 and employed in all the experimental results presented before, at no load and full-load operation. The two other healthy motors were tested at no-load operation, one was a 5.5 kW IE3 IM and the other one a 7.5 kW IE1 IM. It is important to point out that for different powers and also for different efficiency qualities, the diagnostic signals still show small mean values for the healthy cases. For the 5.5 kW IE2 IM, the different load conditions are marked with an 'x' in the figure. Even operating at full load, as motor or generator, the Euclidean norm is remarkably small compared to the faulty cases.

The healthy zone was defined considering the maximum inherent asymmetry obtained by the experimental results, which was $\| \boldsymbol{x}_{\alpha\beta} \|_{\max} = 0.1$ kA/s. As a criterion, the limit of the healthy zone was defined as the double of this value, meaning

$$\lambda = 2 \| \boldsymbol{x}_{\alpha\beta} \|_{\max} = 0.2\,\text{kA/s}. \quad (13)$$

The location of the fault can be determined by the angle of the displacement $\theta_{\boldsymbol{x}_{\alpha\beta}}$. Ideally, the fault displacement is expected to appear at 0°, 120° and 240° for phases *A*, *B* and *C*, respectively. The maximum computed angular error was obtained for one ITF on phase *B*, where the faulty point is located at 110°. Therefore, a limit of ±30° was defined for the diagnosis.

For the FDI method, the mean value of the diagnostic signals is supervised. Once the presence of an ITF is detected, considering the limit presented in (13), the angle $\theta_{\boldsymbol{x}_{\alpha\beta}}$ is computed as in (12) and Table 6 is analysed to identify which phase is the one presenting the ITF.

## 5 Conclusion

A strategy for stator ITFs diagnosis in IMs based on a zero-sequence signal injection was presented. The injection of the zero-sequence signal can be easily implemented, because it does not require modifying the space vector modulation of the inverter. The injected signal is inherently produced by the PWM at the switching frequency, it does not interact with the current controller and does not produce any additional audible noise. A drawback of the strategy is that it requires access to the neutral point of the IM, nevertheless some position estimation techniques use the access to the neutral point as part of sensorless strategy and can be combined with our ITF diagnosis strategy. This proposal could be suitable for machines driving critical loads, as electric vehicles.

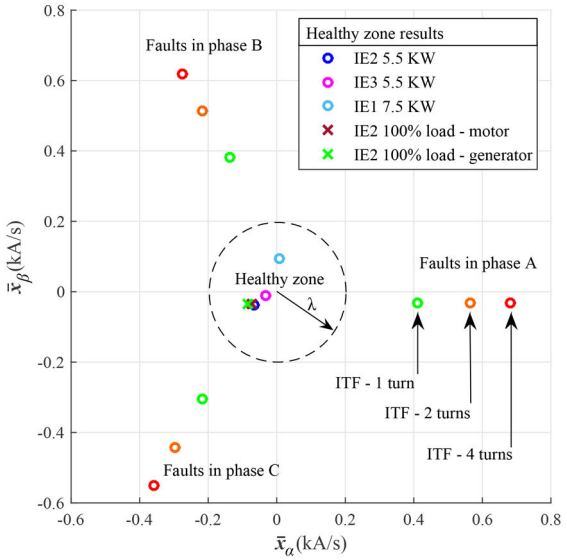


**Fig. 14** *$\bar{x}_\alpha$ versus $\bar{x}_\beta$ in the αβ-plane for different operating conditions, ITF severities and locations. Also results for different healthy IM are shown*

**Table 6** Location of the faulty phase

| | Angle range | Faulty phase |
|---|---|---|
| $\theta_{\boldsymbol{x}_{\alpha\beta}}$ | $0 \pm 30°$ | A |
| $\theta_{\boldsymbol{x}_{\alpha\beta}}$ | $120 \pm 30°$ | B |
| $\theta_{\boldsymbol{x}_{\alpha\beta}}$ | $240 \pm 30°$ | C |

This proposal is able to detect very low severity stator ITFs, such as faults under 1%, which is considered a difficult task. In this work, a single inter-turn short-circuit was accurately detected, which represents 0.6% of the phase winding. We proved the technique is robust, providing good results with the IM operating under time-variable load and time-variable speed conditions. In addition, it was demonstrated that it is possible to detect the location of the fault by analysing the displacement of the diagnostic signals. Different healthy motors were tested, which allowed us to define a healthy zone. This points out that the ITF diagnosis strategy does not need previous knowledge about the machine state or its parameters to determine its condition.

## 6 Acknowledgments

This work was supported by the ANPCyT, CONICET, the Science & Technology Cooperation Programme between MINCyT in Argentina and BMBF in Germany, and the German Academic Exchange Service (DAAD).

## 7 References

[1] Zhang, P., Du, Y., Habetler, T.G., *et al.*: 'A survey of condition monitoring and protection methods for medium-voltage induction motors', *IEEE Trans. Ind. Appl.*, 2011, **47**, (1), pp. 34–46

[2] Kia, S.H., Henao, H., Capolino, G.: 'Survey of real-time fault diagnosis techniques for electromechanical systems'. 2017 IEEE Workshop on Electrical Machines Design, Control and Diagnosis (WEMDCD), Nottingham, United Kingdom, 2017, pp. 290–297

[3] Faiz, J., Ghorbanian, V., Joksimovic, G.: *'Fault diagnosis of induction motors'. Energy engineering* (Institution of Engineering and Technology, UK, 2017)

[4] Lahoud, N., Faucher, J., Malec, D., *et al.*: 'Electrical aging of the insulation of low-voltage machines: model definition and test with the design of experiments', *IEEE Trans. Ind. Electron.*, 2013, **60**, (9), pp. 4147–4155

[5] Muxiri, A.C.P., Bento, F., Fonseca, D.S.B., *et al.*: 'Thermal analysis of an induction motor subjected to inter-turn short-circuit failures in the stator windings'. 2019 Int. Conf. on Industrial Engineering, Applications and Manufacturing (ICIEAM), Sochi, Russia, 2019, pp. 1–5

[6] Faiz, J., Nejadi-Koti, H., Valipour, Z.: 'Comprehensive review on inter-turn fault indexes in permanent magnet motors', *IET Electr. Power Appl.*, 2017, **11**, (1), pp. 142–156

[7] Grubic, S., Aller, J.M., Lu, B., *et al.*: 'A survey on testing and monitoring methods for stator insulation systems of low-voltage induction machines

focusing on turn insulation problems', *IEEE Trans. Ind. Electron.*, 2008, **55**, (12), pp. 4127–4136
[8] Ghanbari, T.: 'Autocorrelation function-based technique for stator turn-fault detection of induction motor', *IET Sci., Meas. Technol.*, 2016, **10**, (2), pp. 100–110
[9] Drif, M., Cardoso, A.J.M.: 'Stator fault diagnostics in squirrel cage three-phase induction motor drives using the instantaneous active and reactive power signature analyses', *IEEE Trans. Ind. Inf.*, 2014, **10**, (2), pp. 1348–1360
[10] Bossio, G.R., De Angelo, C.H., Bossio, J.M., *et al.*: 'Separating broken rotor bars and load oscillations on im fault diagnosis through the instantaneous active and reactive currents', *IEEE Trans. Ind. Electron.*, 2009, **56**, (11), pp. 4571–4580
[11] Mazzoletti, M.A., Bossio, G.R., De Angelo, C.H., *et al.*: 'A model-based strategy for interturn short-circuit fault diagnosis in pmsm', *IEEE Trans. Ind. Electron.*, 2017, **64**, (9), pp. 7218–7228
[12] Abdallah, H., Benatman, K.: 'Stator winding inter-turn short-circuit detection in induction motors by parameter identification', *IET Electr. Power Appl.*, 2017, **11**, (2), pp. 272–288
[13] Irhoumah, M., Mercier, D., Pusca, R., *et al.*: 'Information fusion of external flux sensors for detection of inter-turn short circuit faults in induction machines'. IECON 2017 - 43rd Annual Conf. of the IEEE Industrial Electronics Society, Beijing, China, 2017, pp. 8076–8081
[14] Wang, B., Shen, C., Xu, K., *et al.*: 'Turn-to-turn short circuit of motor stator fault diagnosis in continuous state based on deep auto-encoder', *IET Electr. Power Appl.*, 2019, **13**, (10), pp. 1598–1606
[15] Akhil Vinayak, B., Anjali Anand, K., Jagadanand, G.: 'Wavelet-based real-time stator fault detection of inverter-fed induction motor', *IET Electr. Power Appl.*, 2020, **14**, (1), pp. 82–90
[16] Frosini, L.: 'Monitoring and diagnostics of electrical machines and drives: a state of the art'. 2019 IEEE Workshop on Electrical Machines Design, Control and Diagnosis (WEMDCD), Athens, Greece, vol. 1, 2019, pp. 169–176
[17] Xu, P., Zhu, Z.Q.: 'Analysis of parasitic effects in carrier signal injection methods for sensorless control of pm synchronous machines', *IET Electr. Power Appl.*, 2018, **12**, (2), pp. 203–212
[18] Samonig, M.A., Wolbank, T.M.: 'Exploiting rotor slotting harmonics to determine and separate static and dynamic air-gap eccentricity in induction machines'. 2017 IEEE 11th Int. Symp. on Diagnostics for Electrical Machines, Power Electronics and Drives (SDEMPED), Tinos, Greece, 2017, pp. 52–57
[19] Bossio, G.R., De Angelo, C.H., Garcia, G.O., *et al.*: 'Effects of rotor bar and end-ring faults over the signals of a position estimation strategy for induction motors', *IEEE Trans. Ind. Appl.*, 2005, **41**, (4), pp. 1005–1012
[20] Briz, F., Degner, M.W., Guerrero, J.M., *et al.*: 'Stator windings fault diagnostics of induction machines operated from inverters and soft-starters using high-frequency negative-sequence currents', *IEEE Trans. Ind. Appl.*, 2009, **45**, (5), pp. 1637–1646
[21] Briz, F., Degner, M.W., Diez, A.B., *et al.*: 'Online diagnostics in inverter-fed induction machines using high-frequency signal injection', *IEEE Trans. Ind. Appl.*, 2004, **40**, (4), pp. 1153–1161
[22] Yang, S.C.: 'Online turn fault detection of interior permanent-magnet machines using the pulsating-type voltage injection', *IEEE Trans. Ind. Appl.*, 2016, **52**, (3), pp. 2340–2349
[23] Du, B., Wu, S., Han, S., *et al.*: 'Interturn fault diagnosis strategy for interior permanent-magnet synchronous motor of electric vehicles based on digital signal processor', *IEEE Trans. Ind. Electron.*, 2016, **63**, (3), pp. 1694–1706
[24] Arellano-Padilla, J., Sumner, M., Gerada, C.: 'Evaluation of saliency tracking as an alternative for health monitoring in pmsm-drives under non-stationary conditions', *IET Electr. Power Appl.*, 2016, **10**, (4), pp. 284–293
[25] Stojičić, G., Stanković, J., Joksimović, G., *et al.*: 'Increasing sensitivity of stator winding short circuit fault indicator in inverter fed induction machines'. 2012 15th Int. Power Electronics and Motion Control Conf. (EPE/PEMC), Novi Sad, Serbia, 2012, pp. DS2a.10-1–DS2a.10-6
[26] Arellano-Padilla, J., Sumner, M., Gerada, C.: 'Condition monitoring approach for permanent magnet synchronous motor drives based on the inform method', *IET Electr. Power Appl.*, 2016, **10**, (1), pp. 54–62
[27] Bossio, G.R., De Angelo, C.H., de la Barrera, P.M., *et al.*: 'Stator winding fault detection in induction motor drives using signal injection'. 8th IEEE Symp. on Diagnostics for Electrical Machines, Power Electronics Drives, Belogna, Italy, 2011, pp. 92–97
[28] Sen, B., Wang, J.: 'Stator interturn fault detection in permanent-magnet machines using pwm ripple current measurement', *IEEE Trans. Ind. Electron.*, 2016, **63**, (5), pp. 3148–3157
[29] Liu, H., Huang, J., Hou, Z., *et al.*: 'Stator inter-turn fault detection in closed-loop controlled drive based on switching sideband harmonics in cmv', *IET Electr. Power Appl.*, 2017, **11**, (2), pp. 178–186
[30] Otero, M., Bossio, G.R., de la Barrera, P.M., *et al.*: 'Interturn faults detection in induction motor drives using zero-sequence signal injection'. 2018 Int. Symp. on Power Electronics, Electrical Drives, Automation and Motion (SPEEDAM), Amalfi, Italy, 2018, pp. 202–207
[31] Bossio, G.R., de la Barrera, P.M., Otero, M., *et al.*: 'Broken rotor bars detection in induction motor by using zero-sequence signal injection'. IECON 2016 - 42nd Annual Conf. of the IEEE Industrial Electronics Society, Florence, Italy, 2016, pp. 1482–1487
[32] Otero, M., de la Barrera, P.M., Bossio, G.R., *et al.*: 'A strategy for broken bars diagnosis in induction motors drives', *IEEE Latin Am. Trans.*, 2018, **16**, (2), pp. 322–328
[33] Cheng, S., Zhang, P., Habetler, T.G.: 'An impedance identification approach to sensitive detection and location of stator turn-to-turn faults in a closed-loop multiple-motor drive', *IEEE Trans. Ind. Electron.*, 2011, **58**, (5), pp. 1545–1554
[34] Xu, P.L., Zhu, Z.Q.: 'Novel carrier signal injection method using zero-sequence voltage for sensorless control of pmsm drives', *IEEE Trans. Ind. Electron.*, 2016, **63**, (4), pp. 2053–2061
[35] Gyftakis, K.N., Marques-Cardoso, A.J.: 'Reliable detection of very low severity level stator inter-turn faults in induction motors'. IECON 2019 - 45th Annual Conf. of the IEEE Industrial Electronics Society, Lisbon, Portugal, vol. 1, 2019, pp. 1290–1295
[36] Briz, F., Degner, M.W., Garcia, P., *et al.*: 'Rotor position estimation of ac machines using the zero-sequence carrier-signal voltage', *IEEE Trans. Ind. Appl.*, 2005, **41**, (6), pp. 1637–1646
[37] Tousizadeh, M., Che, H.S., Selvaraj, J., *et al.*: 'Fault-tolerant field-oriented control of three-phase induction motor based on unified feedforward method', *IEEE Trans. Power Electron.*, 2019, **34**, (8), pp. 7172–7183
[38] Leidhold, R.: 'Position sensorless control of pm synchronous motors based on zero-sequence carrier injection', *IEEE Trans. Ind. Electron.*, 2011, **58**, (12), pp. 5371–5379
[39] Zhao, Z., Horn, B., Leidhold, R.: 'Investigation of common-mode current elimination in four-wire inverter-fed motor'. 2018 IEEE Int. Power Electronics and Application Conf. and Exposition (PEAC), Shenzhen, China, 2018, pp. 1–5
[40] Krause, P.C., Wasynczuk, O., Sudhoff, S.D., *et al.*: '*Analysis of electric machinery and drive systems*' (IEEE Press, New York, USA, 2013, 3rd edn)
[41] de la Barrera, P.M., Bossio, G.R., Leidhold, R.: 'Induction motor saliencies analysis using zero-sequence signal injection'. 2015 IEEE 24th Int. Symp. on Industrial Electronics (ISIE), Buzios, Brazil, 2015, pp. 518–523
[42] Wolbank, T.M., Machl, J.L., Hauser, H.: 'Closed-loop compensating sensors versus new current derivative sensors for shaft-sensorless control of inverter fed induction machines', *IEEE Trans. Instrum. Meas.*, 2004, **53**, (4), pp. 1311–1315
[43] Holtz, J., Juliet, J.: 'Sensorless acquisition of the rotor position angle of induction motors with arbitrary stator windings', *IEEE Trans. Ind. Appl.*, 2005, **41**, (6), pp. 1675–1682
[44] Briz, F., Degner, M.W.: 'Rotor position estimation', *IEEE Ind. Electron. Mag.*, 2011, **5**, (2), pp. 24–36
[45] WEG.Group. 'Induction motors fed by pwm frequency inverters, technical guide', 2018
[46] Arora, T.G., Aware, M.V., Tutakne, D.R.: 'Effect of pulse width modulated voltage on induction motor insulation'. 2012 7th IEEE Conf. on Industrial Electronics and Applications (ICIEA), Singapore, 2012, pp. 2044–2048
[47] Melfi, M.J.: 'Low-voltage pwm inverter-fed motor insulation issues', *IEEE Trans. Ind. Appl.*, 2006, **42**, (1), pp. 128–133
[48] Tallam, R.M., Habetler, T.G., Harley, R.G.: 'Transient model for induction machines with stator winding turn faults', *IEEE Trans. Ind. Appl.*, 2002, **38**, (3), pp. 632–637